Supporting Information for:

Trapping of an Ni^{II} sulfide by a Co^{I} fulvene complex

Nathaniel J. Hartmann, Guang Wu, and Trevor W. Hayton*

[a] Department of Chemistry and Biochemistry, University of California Santa Barbara, Santa Barbara CA 93106

*To whom correspondence should be addressed. Email: hayton@chem.ucsb.edu

Table of Contents

Experimental Details	S3
NMR Spectra	S4
X-ray Crystallographic Data	S12
IR Spectra	S14
UV-Vis	S15
Electrochemistry	S16
References	S19

Experimental

NMR scale reaction of [$L^{tBu}Ni^{II}(SCPh_3)$] with Cp^*_2Co in THF-d_8 to determine yield of unidentified Ni(I) product. To a 20 mL scintillation vial containing [$L^{tBu}Ni^{II}(SCPh_3)$] (19.7 mg, 0.0235 mmol) and HMDSO (5 μL, 0.0235 mmol) in cold, stirring THF-d_8 (0.3 mL) was added dropwise a solution of Cp^*_2Co (15.5 mg, 0.0470 mmol) in THF-d_8 (0.3 mL). After addition, the color of the solution quickly changed from blue to red-brown. The solution was then transferred to an NMR tube. A ^{1}H NMR spectrum taken after 4 h revealed the presence of resonances assignable to **3**, **1**, the unidentified Ni^I-containing product, and free Cp^*_2Co. Integration of the peaks assigned to complex **1** and the unidentified Ni^I-containing product revealed that they are present in an approximately 5:2 ratio (Figure S8). ^{1}H NMR (400 MHz, 25 °C, THF-d_8): δ 20.0 (overlapping br s, **1** and **I**), 11.70 (br s, Cp^*_2Co), 7.3-7.05 (15 H, $HCPh_3$, Ar-**H**), 6.14 (s, **2**), 5.56 (s, 1H, **H**CPh_3), 3.5 (br s, **1**), 2.6 (br s, 2H, **3**, C**H**$_2$), 1.5 (br s, 15H, **3**, Cp* C**H**$_3$), 1.4 (br s, **1**), 0.2 (br s, **I**), 0.07 (HMDSO), -1.3 (br s, **1**), -1.6 (br s, **I**), -11.9 (overlapping br s, **1** and **I**).

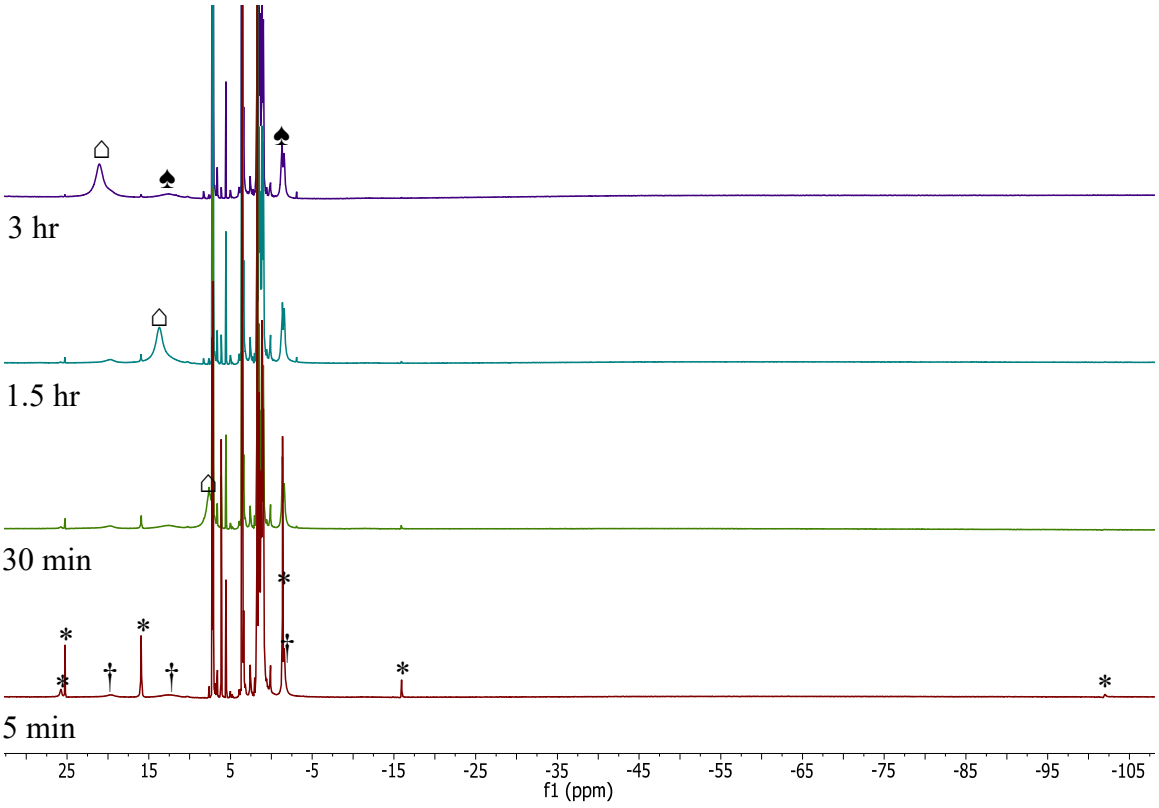

Figure S1. ^{1}H NMR spectra of the reaction of [L^{tBu}Ni(SCPh$_3$)] with two equiv. of Cp*$_2$Co in THF-d_8. (*) indicates the presence of **2**, (⌂) indicates the presence of Cp*$_2$Co, (†) indicates the presence of an unknown Ni^{I}-containing product, and (♠) indicates the presence of **1**.

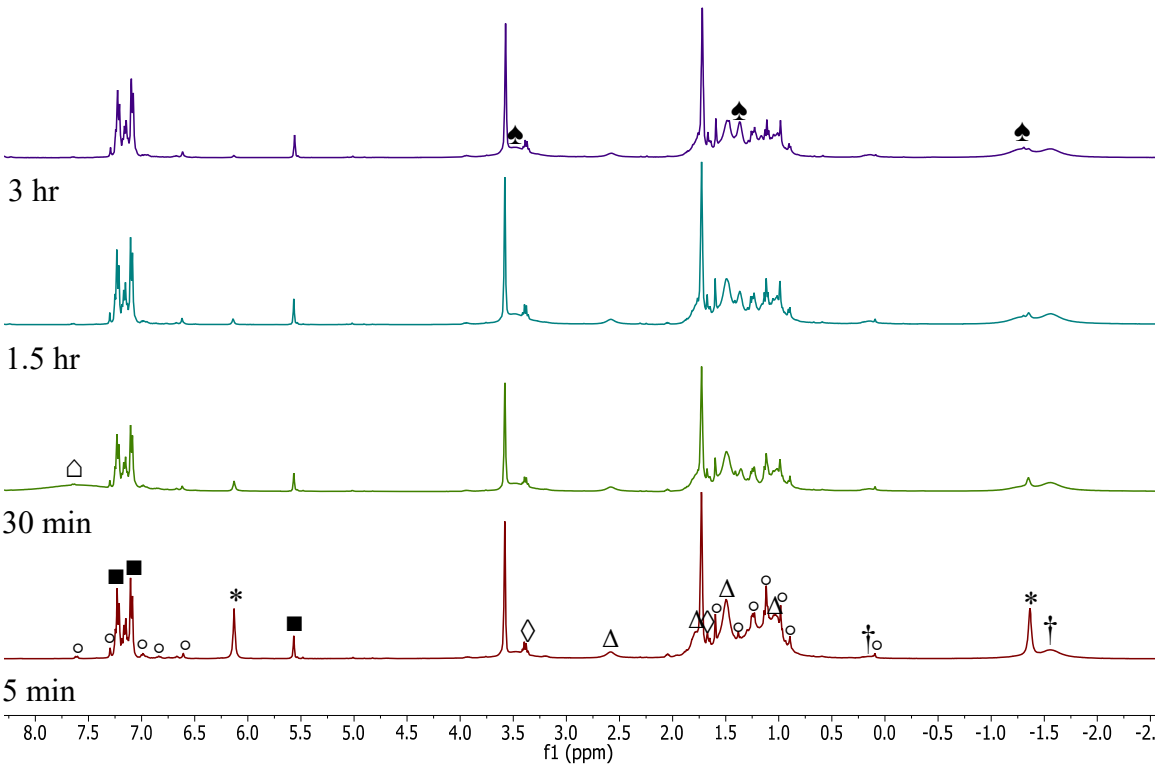

Figure S2. Partial ^{1}H NMR spectra of the reaction of [L^{tBu}Ni(SCPh$_3$)] with two equiv. of Cp*$_2$Co in THF-d_8. (*) indicates the presence of **2**, (Δ) indicates the presence of **3**, (♠) indicates the presence of **1**, (⌂) indicates the presence of Cp*$_2$Co, (■) indicates the presence of HCPh$_3$, (†) indicates the presence of an unidentified Ni^{I}-containing product, (◊) indicates the presence of Et$_2$O, and (°) indicates the presence of unidentified decomposition products.

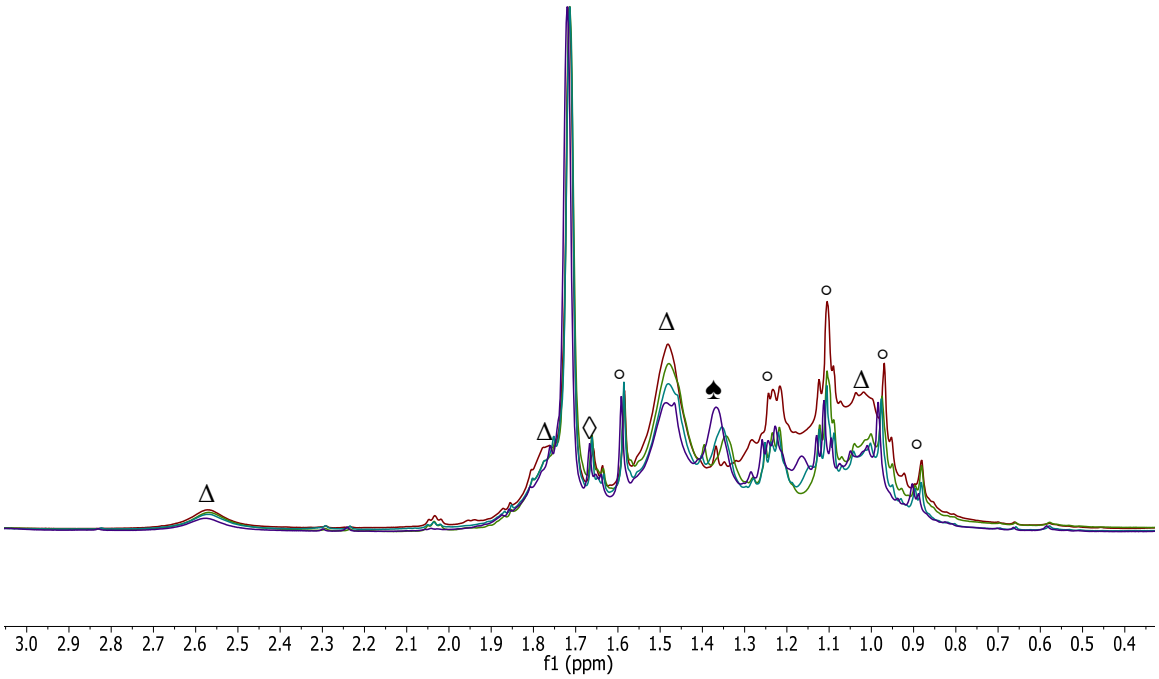

Figure S3. Partial ^{1}H NMR spectra of the reaction of [L^{tBu}Ni(SCPh$_3$)] with two equiv. of Cp*$_2$Co in THF-d_8: red (5 min), green (30 min), cyan (1.5 h), and purple (3 h). (Δ) indicates the presence of **3**, (♠) indicates the presence of **1**, (◊) indicates the presence of Et_2O, and (°) indicates the presence of unidentified decomposition product. These spectra, which are normalized to the THF-d_8 resonance at 1.72 ppm, clearly demonstrate a decrease in the intensity of the peaks assignable to complex **3** as the reaction progresses. It is important to note, however, that, because of the formation of the unidentified Ni(I) by-product, we do not expect full consumption of complex **3** during this reaction.

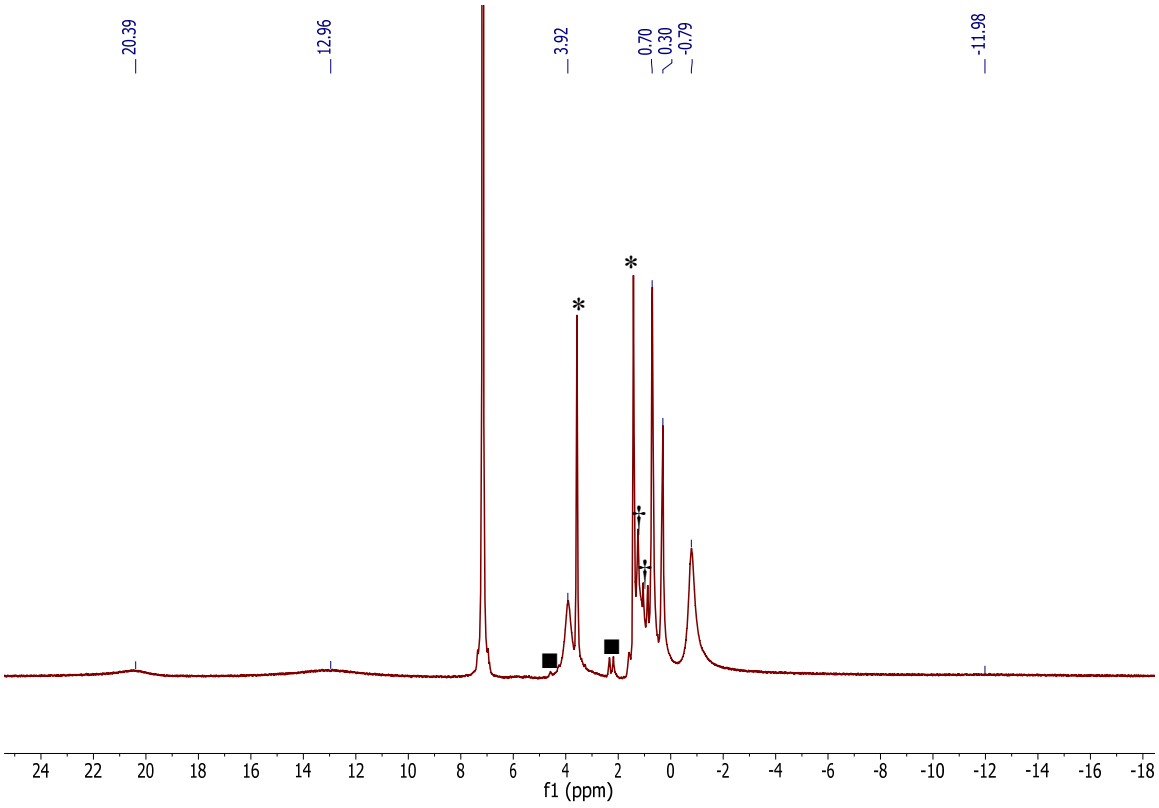

Figure S4. ^{1}H NMR spectrum of **1** in C_6D_6. (*) indicates the presence THF, (†) indicates the presence of pentane, (■) indicates the presence of an unidentified impurity.

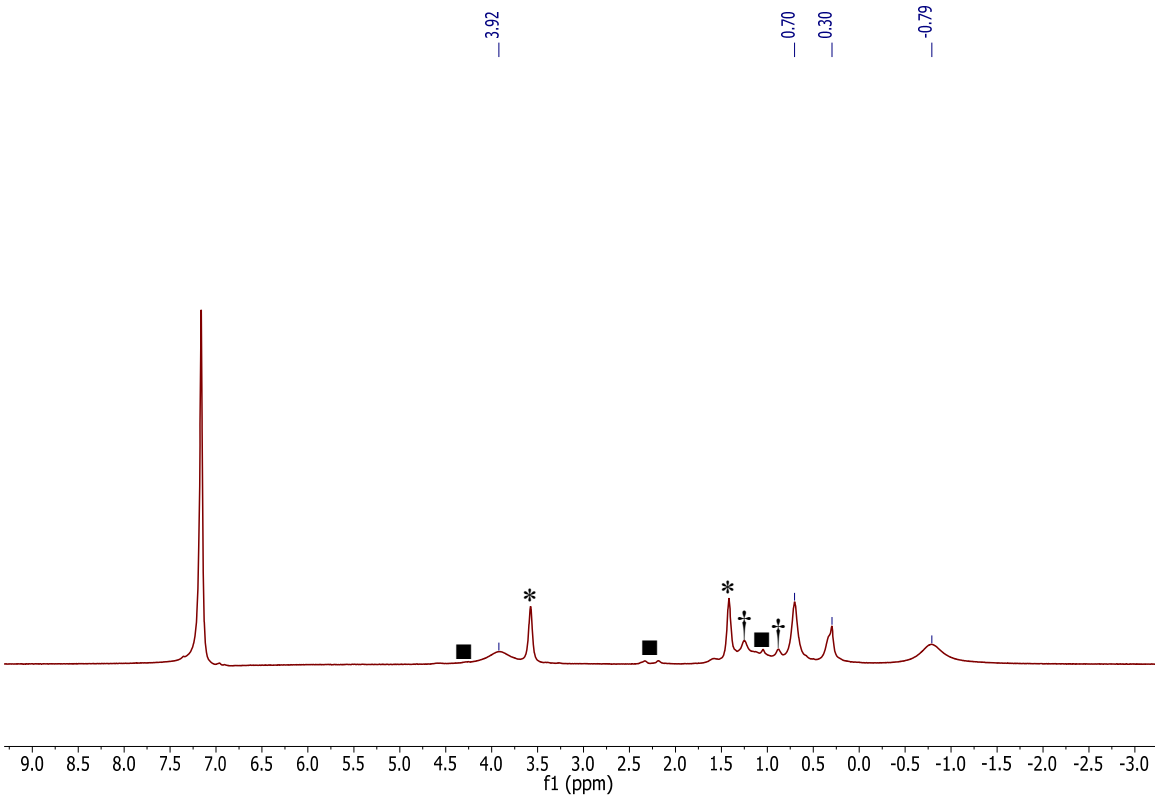

Figure S5. Partial ^{1}H NMR spectrum of **1** in C_6D_6. (*) indicates the presence THF, (†) indicates the presence of pentane, (■) indicates the presence of an unidentified impurity.

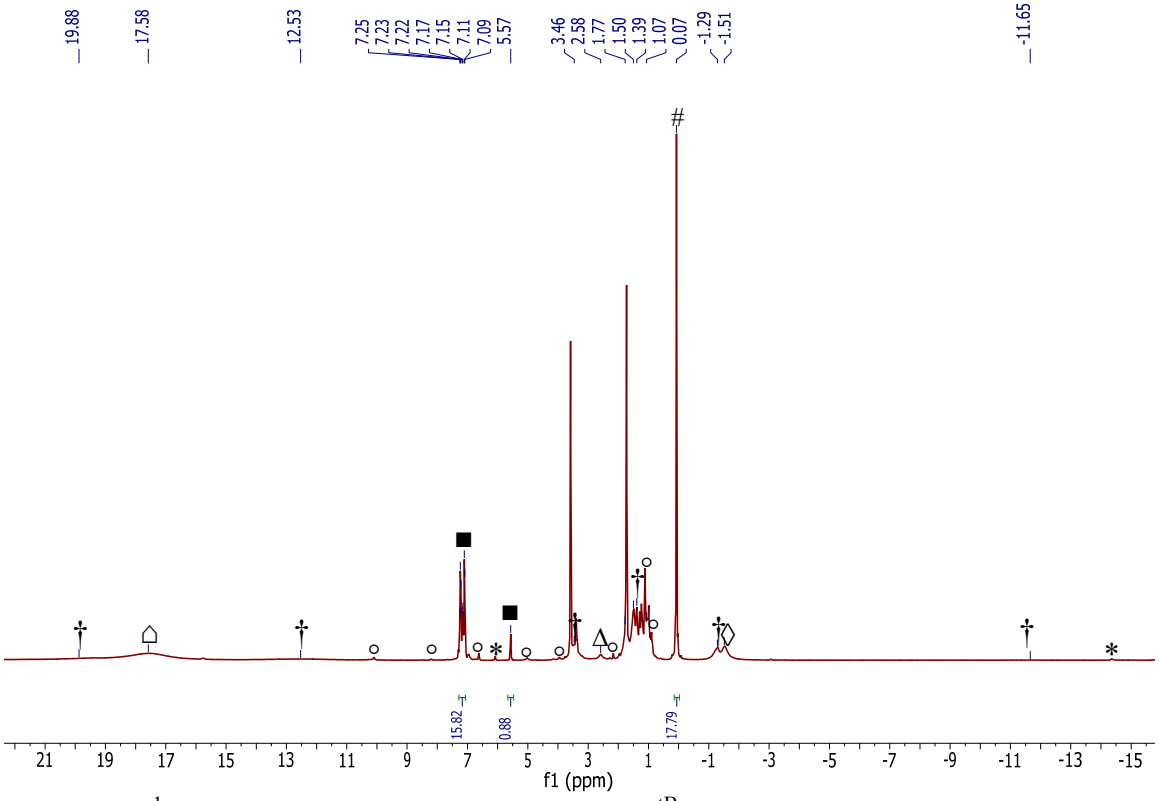

Figure S6. ^{1}H NMR spectrum of the reaction of [L^{tBu}Ni(SCPh$_3$)] with two equiv. of Cp*$_2$Co in THF-d_8 with HMDSO as an internal standard. (†) indicates the presence of **1**, (■) indicates the presence of HCPh$_3$, (Δ) indicates the presence of **3**, (⌂) indicates the presence of Cp*$_2$Co, (◊) indicates the presence of an unidentified Ni^{I}-containing product, (#) indicates the presence HMDSO, (*) indicates the presence of **2**, and (°) indicates the presence of unidentified decomposition products.

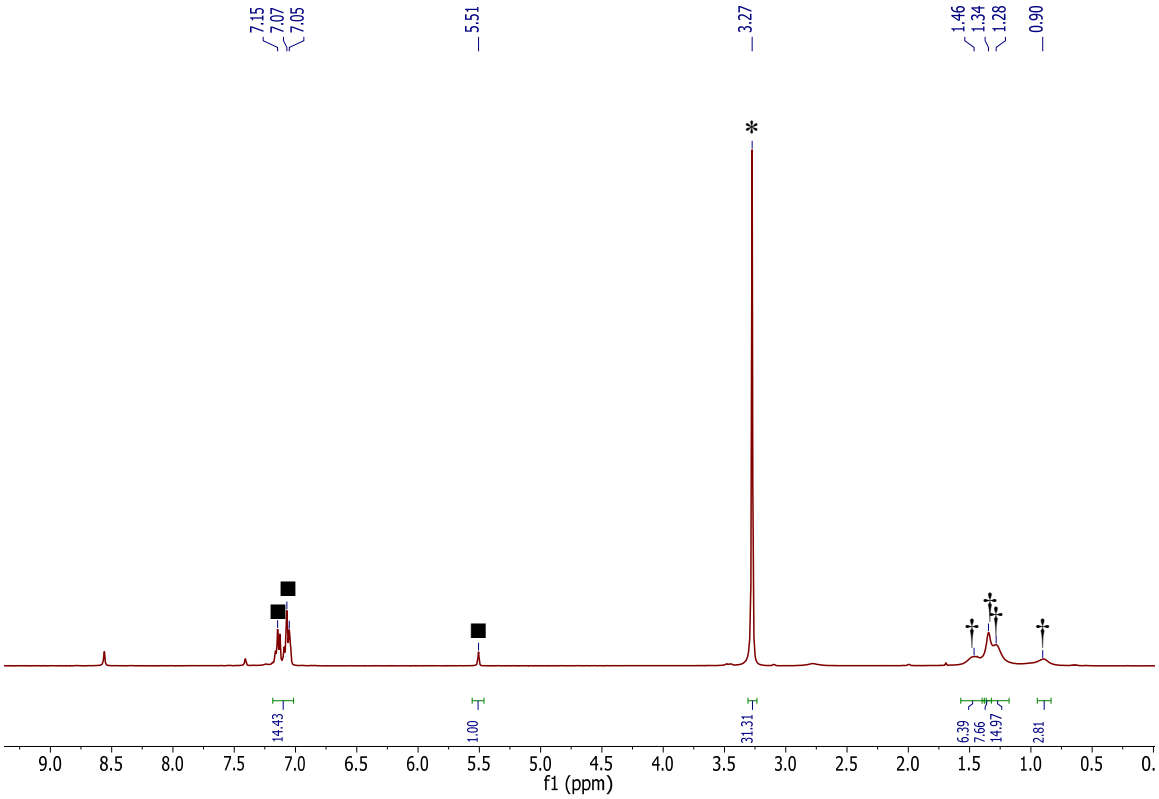

Figure S7. ^{1}H NMR spectrum of the reaction of [Cp*$_2$Co][PF_6] and [K(18-crown-6)][CPh_3] in pyridine-d_5. (*) indicates the presence of 18-crown-6, (†) indicates the presence of **3**, (■) indicates the presence of $HCPh_3$.

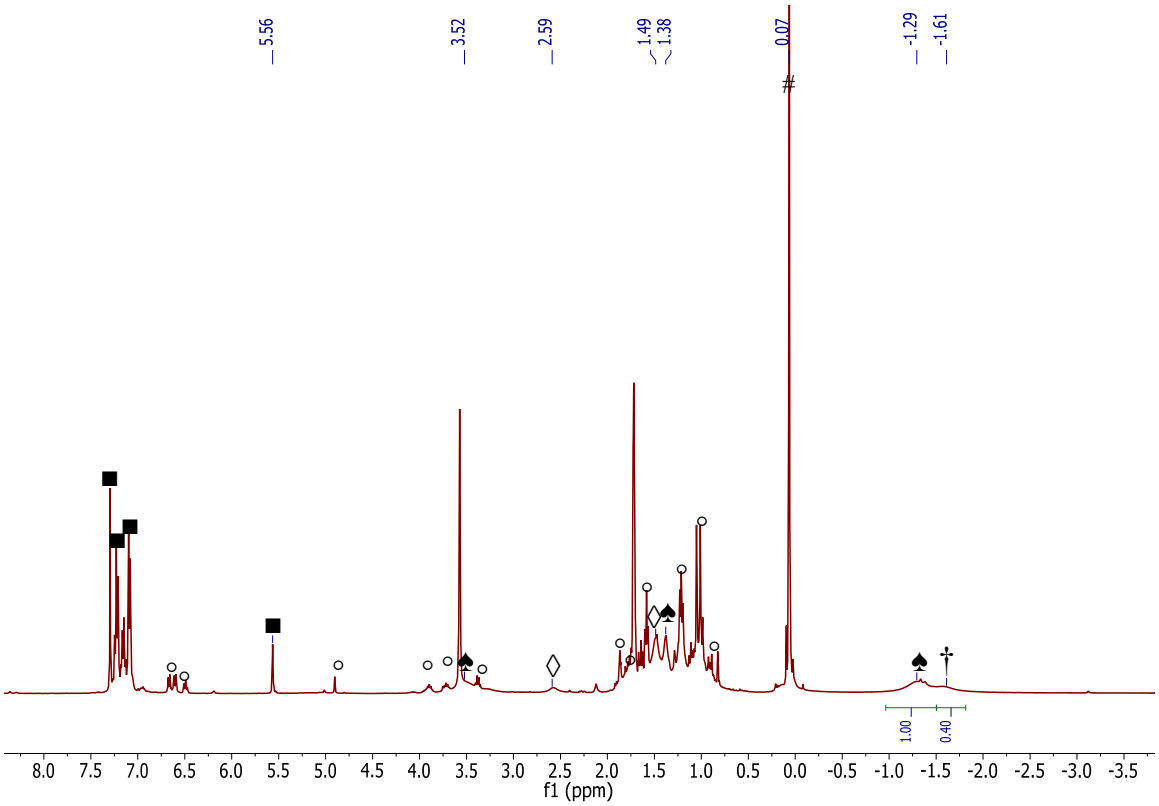

Figure S8. Partial ^{1}H NMR spectra of the reaction of [L^{tBu}Ni(SCPh$_3$)] with two equiv. of Cp*$_2$Co in THF-d_8. (†) indicates the presence of an unknown Ni^{I} product, (■) indicates the presence of HCPh$_3$, (#) indicates the presence HMDSO, (♠) indicates the presence of **1**, (◊) indicates the presence of **3**, and (°) indicates the presence of unidentified decomposition products.

X-ray Crystallography. Data for complex **1**·$C_4H_{10}O$ was collected on a Bruker KAPPA APEX II diffractometer equipped with an APEX II CCD detector using a TRIUMPH monochromator with a Mo Kα X-ray source (α = 0.71073 Å). The crystals were mounted on a cryoloop under Paratone-N oil, and all data were collected at 100(2) K using an Oxford nitrogen gas cryostream. Data were collected using ω scans with 0.5° frame widths and frame exposures of 20 seconds. Data collection and cell parameter determination were conducted using the SMART program.[1] Integration of the data frames and final cell parameter refinement were performed using SAINT software.[2] Absorption correction of the data was carried out using the multi-scan method SADABS.[3] Subsequent calculations were carried out using SHELXTL.[4] Structure determination was done using the direct method and difference Fourier techniques. All hydrogen atom positions were idealized, and rode on the atom of attachment. Structure solution, refinement, graphics, and creation of publication materials were performed using SHELXTL.[4]

Further crystallographic details for complex **1**·$C_4H_{10}O$ can be found in Table S1.

Table S1. X-ray Crystallographic Data for complex **1**·$C_4H_{10}O$.

	1·$C_4H_{10}O$
empirical formula	$C_{55}H_{82}CoN_2NiS$, $C_4H_{10}O$
crystal habit, color	Plate, Brown
crystal size (mm)	0.25 × 0.10 × 0.05
crystal system	Monoclinic
space group	*P21/c*
volume (Å^3)	5546.8(7)
a (Å)	12.2784(8)
b (Å)	25.957(2)
c (Å)	17.836(1)
α (deg)	90
β (deg)	102.645(5)
γ (deg)	90
Z	4
formula weight (g/mol)	995.04
density (calculated) (Mg/m^3)	1.192
absorption coefficient (mm^{-1})	0.715
F_{000}	2156
total no. reflections	11410
unique reflections	5043
R_{int}	0.1760
final R indices (I >2σ(I)]	R_1 = 0.0802 wR_2 = 0.1283
largest diff. peak and hole (e$^-$ A^{-3})	1.217 and -0.684
GOF	0.984

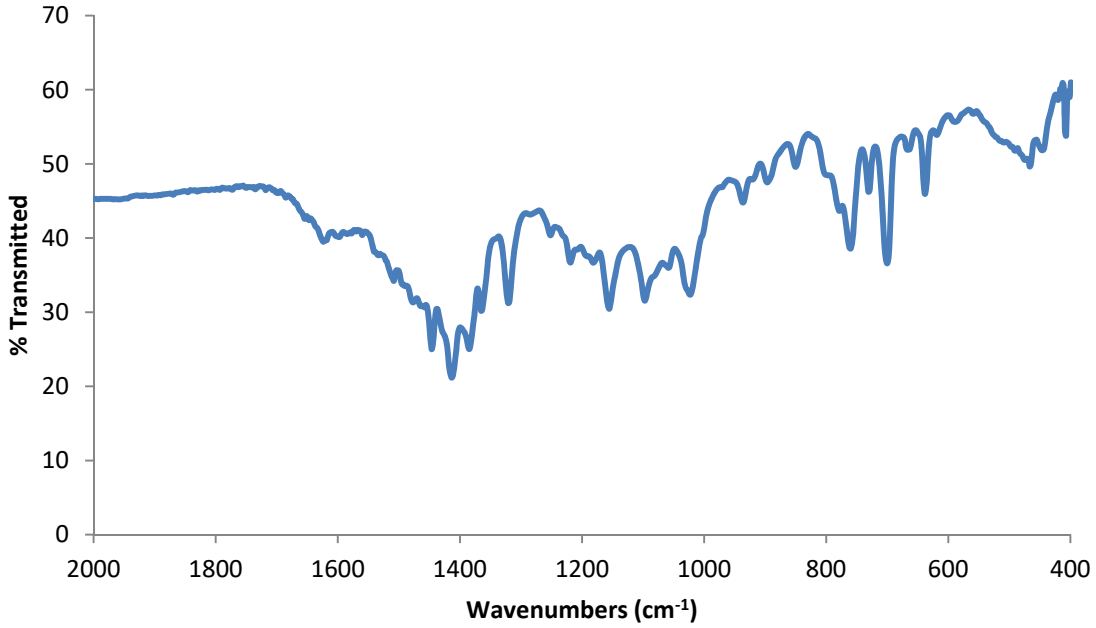

Figure S11. Partial IR spectrum of complex **1** (KBr pellet).

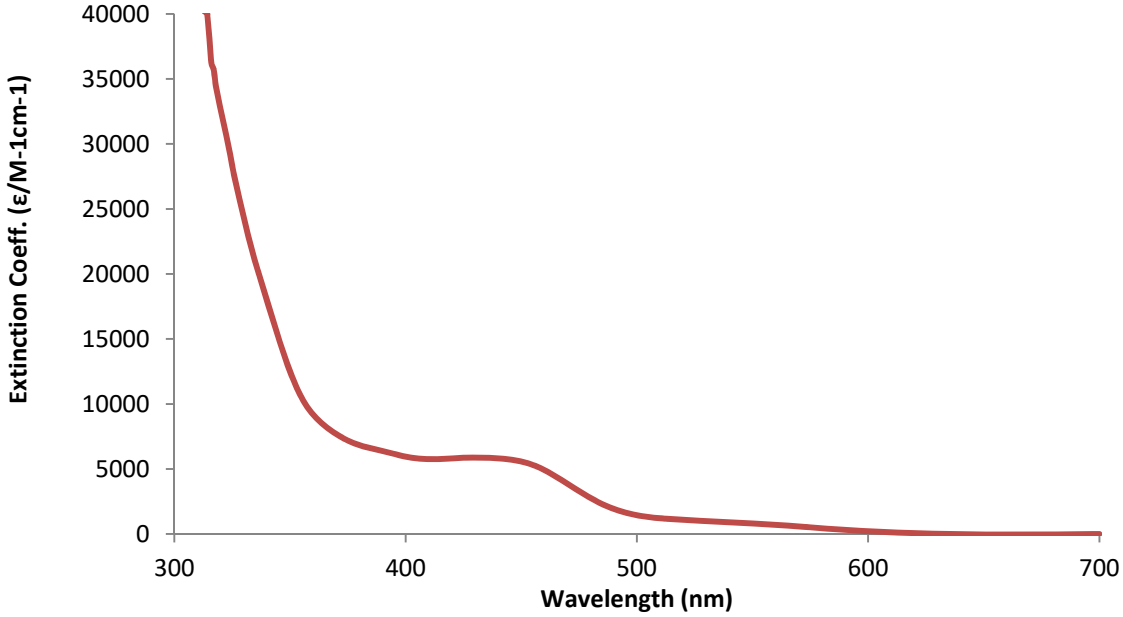

Figure S12. UV-vis spectrum of complex **1** (1.0 mM in C_6H_6).

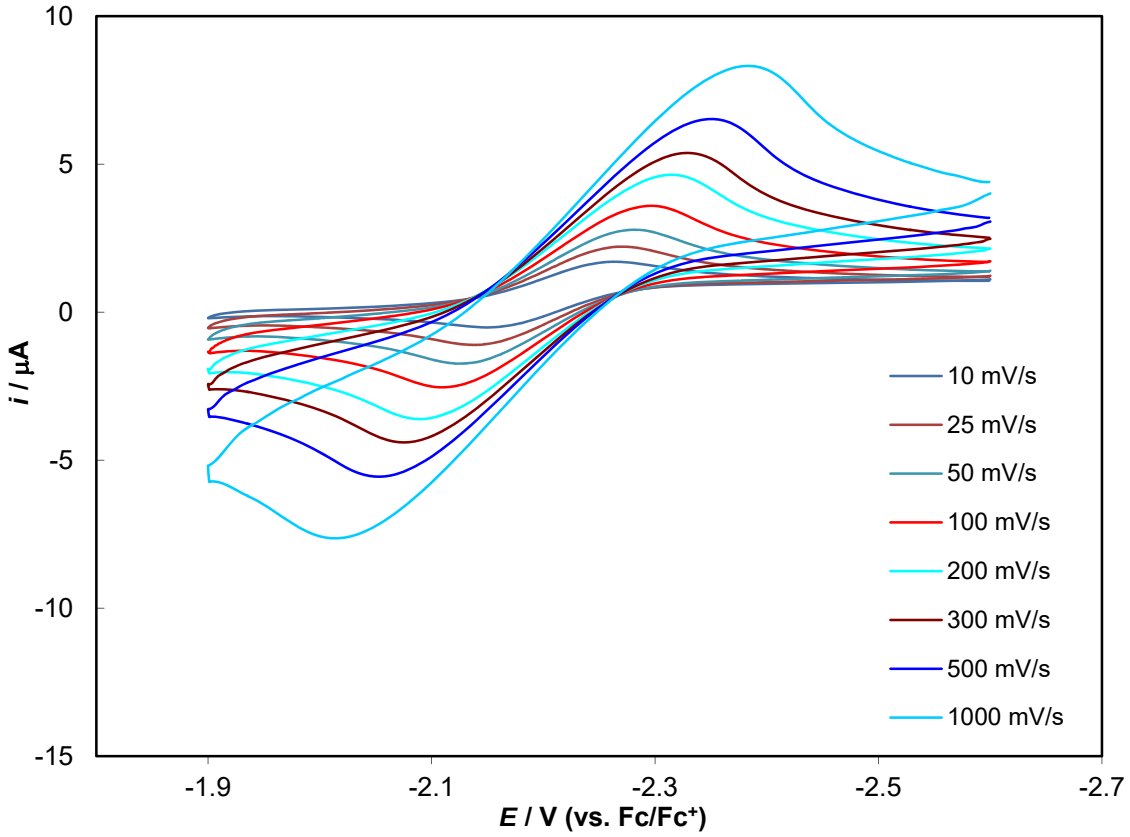

Figure S13. Cyclic voltammogram of the Co(III)/Co(II) redox feature of complex **1** measured in THF with 0.1 M $[NBu_4][PF_6]$ as the supporting electrolyte (vs. Fc/Fc^+).

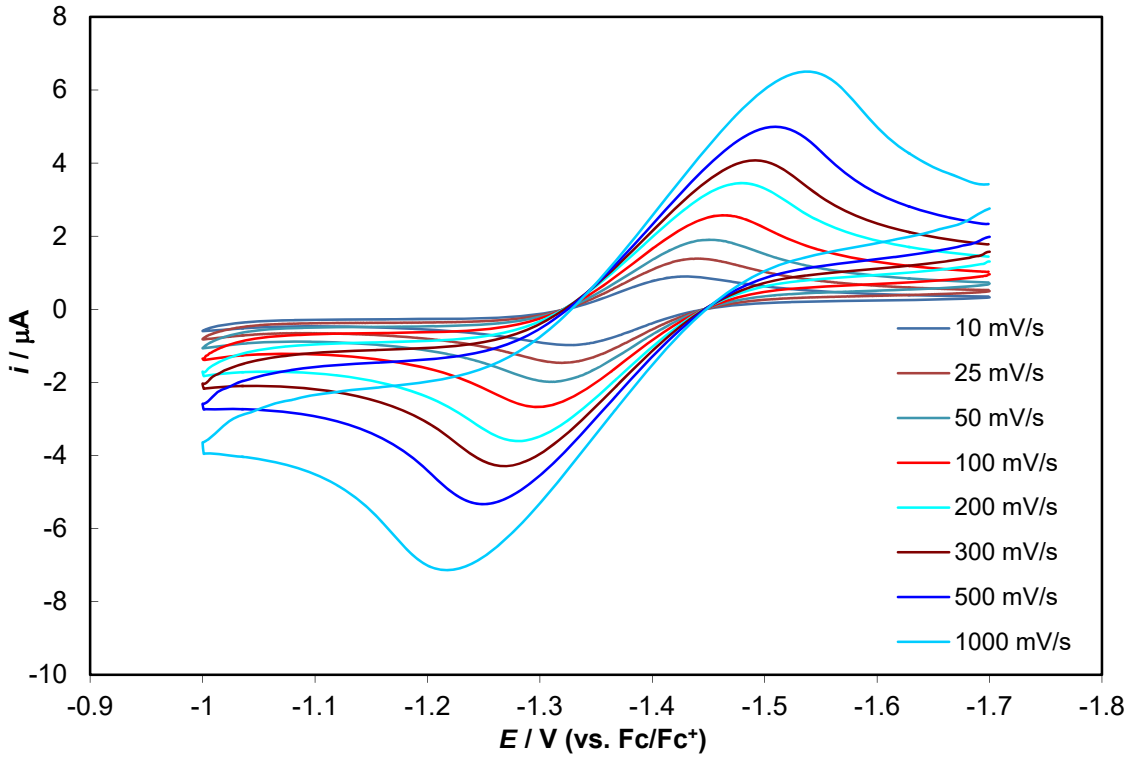

Figure S14. Cyclic voltammogram of the Ni(II)/Ni(I) redox feature of complex **1** measured in THF with 0.1 M $[NBu_4][PF_6]$ as the supporting electrolyte (vs. Fc/Fc^+).

Table S2. Electrochemical parameters for [$L^{tBu}Ni^{I}(SCH_2Me_4C_5)Co(Cp^*)$] (**1**) in THF (vs. Fc/Fc^+, $[NBu_4][PF_6]$ as the supporting electrolyte).

Co(III)/Co(II) Feature	**Scan rate, V/s**	**$E_{p,c}$, V**	**$E_{p,a}$, V**	**ΔE_p[a]**	**$i_{p,a}/i_{p,c}$**
	0.010	-2.264	-2.150	0.114	0.99
	0.025	-2.275	-2.139	0.136	1.05
	0.050	-2.281	-2.124	0.157	1.13
	0.100	-2.296	-2.111	0.185	1.21
	0.200	-2.319	-2.094	0.225	1.25
	0.300	-2.329	-2.076	0.253	1.48
	0.500	-2.347	-2.053	0.294	1.46
	1.000	-2.381	-2.021	0.36	1.77
Ni(II)/Ni(I) Feature	**Scan rate, V/s**	**$E_{p,c}$, V**	**$E_{p,a}$, V**	**ΔE_p[a]**	**$i_{p,a}/i_{p,c}$**
	0.010	-1.426	-1.325	0.101	0.94
	0.025	-1.441	-1.314	0.127	0.95
	0.050	-1.446	-1.309	0.137	0.97
	0.100	-1.462	-1.295	0.167	1.00
	0.200	-1.473	-1.280	0.193	1.01
	0.300	-1.490	-1.265	0.225	1.01
	0.500	-1.505	-1.247	0.258	1.01
	1.000	-1.531	-1.220	0.311	1.03

[a] ΔE_p is defined as the potential difference between the anodic wave and the cathodic wave generated after the change in sweep direction.

References

(1) SMART Apex II, Version 2.1, Bruker AXS Inc., Madison, WI, 2005,
(2) SAINT Software User's Guide, Version 7.34a, Bruker AXS Inc., Madison, WI, 2005,
(3) SADABS, Sheldrick, G. M., University of Gottingen, Germany, 2005,
(4) SHELXTL PC, Version 6.12, Bruker AXS Inc., Madison, WI, 2005,